IEEE Access
Multidisciplinary | Rapid Review | Open Access Journal

Received May 30, 2020, accepted June 13, 2020, date of publication June 22, 2020, date of current version July 9, 2020.

Digital Object Identifier 10.1109/ACCESS.2020.3004282

Synthesis and Modification of Cetacean Tonal Sounds for Underwater Bionic Covert Detection and Communication

JIAJIA JIANG[1], (Senior Member, IEEE), ZHONGBO SUN[1], FAJIE DUAN[1], XIAO FU[1], XIANQUAN WANG[1], CHUNYUE LI[1], WEI LIU[2], (Senior Member, IEEE), AND LIN GAN[1], (Member, IEEE)

[1]State Key Lab of Precision Measuring Technology and Instruments, Tianjin University, Tianjin 300072, China
[2]Department of Electronic and Electrical Engineering, The University of Sheffield, Sheffield S10 2TG, U.K.

Corresponding author: Jiajia Jiang (jiajiajiang@tju.edu.cn)

This work was supported in part by the National Natural Science Foundations of China under Grant 61971307, Grant 61905175, and Grant 51775377, in part by the Equipment pre-research field fund under Grant 61405180505 and Grant 61400040303, in part by the Science and Technology on Underwater Information and Control Laboratory under Grant 6142218081811, in part by the Fok Ying Tung Education Foundation under Grant 171055, in part by the National key research and development plan under Grant 2017YFF0204800, in part by the TianJin Natural Science Foundations of China under Grant 17JCQNJC01100, and in part by National Science and Technology Major Project under Grant 2017-V-0009.

ABSTRACT For most conventional bionic signal design methods, they cannot construct high-similarity bionic signals to match those complex cetacean sounds because they are only based on relatively simple bionic signal models. Besides, although very few methods based on the weighted signal superposition technology can construct high-similarity bionic signals, it's very difficult to adjust relevant parameters to match different cetacean sounds or synthesize other desired bionic signals. To solve these problems, firstly, two bionic signal models are proposed individually to mimic cetacean sounds with a simple time-frequency (TF) structure, and then they are combined to mimic cetacean sounds with complex TF structures based on a designed piecewise construction strategy. Based on the two models, the parameters of the synthesized bionic signals can be adjusted to improve detection and communication performance of the bionic signals. The experimental results show that the Pearson correlation coefficient (PCC) results between 13 true cetacean sounds and their corresponding bionic signals are higher than 0.97, and 11 results of them are no less than 0.99. Four key performance indicators of a bionic signal are improved by more than 40% when bandwidth increases by 1kHz. Experimental results demonstrate that the proposed method cannot only efficiently imitate all kinds of simple and complex cetacean tonal sounds with high similarity, but also construct a variety of the same type of bionic signals by simply adjusting model parameters. In addition, the proposed method can also be applied to other areas, such as constructing a new cetacean sound database and so on.

INDEX TERMS Covert, active sonar, underwater acoustic communication, cetacean sound, bionic signal.

I. INTRODUCTION

Owing to sending out signals actively, active sonar detection (ASD) and underwater acoustic communication (UAC) systems can easily be detected by the adversaries. In the last few decades, many methods have been proposed to improve the covertness of sonar signals and underwater communication signals [1]–[6].

Underwater bionic covert detection and communication is a novel approach to realize covert ASD and UAC. Its main idea is to disguise sonar or communication signals into cetacean sounds. During the identification of underwater monitoring systems, these bionic sonar and communication signals could be classified as ocean noise and filtered out [7]–[10], thereby achieving the purpose of covert ASD and UAC. As an approach with great potential, underwater bionic covert detection and communication has been attracting more and more attentions in recent years [11]–[22].

The design of bionic signals is the key to underwater bionic covert detection and communication. More specifically, bionic signals should meet the covertness and the validity requirements (e.g. communication rate, detection

The associate editor coordinating the review of this manuscript and approving it for publication was Jingchang Huang.

accuracy etc.) for covert ASD and UAC systems. However, the covertness of ASD and UAC systems depends on the camouflage ability of bionic signals.

The design of bionic signals includes signal synthesis and modification. To ensure the camouflage ability, in the synthesis of bionic signals, it is necessary to match the acoustic characteristics of bionic signals, such as waveform shape, frequency distribution and time-frequency (TF) distribution, to that of cetacean sounds as closely as possible. However, the bionic signals with high camouflage ability do not necessarily meet the validity requirements of ASD and UAC. Therefore, efficient signal models and corresponding signal construction methods are very important for efficiently and effectively imitating all kinds of simple and complex cetacean tonal sounds.

In addition, synthesis and modification of bionic signals also play an important role in other areas. For example, efficient synthesis and modification models and methods of bionic signals can be used to construct a new cetacean sounds database based on existing ones [23], and construct all kinds of bionic signals to simulate cetaceans and then evaluate the behaviour impact of different acoustic characteristics on cetaceans [24].

There has been some progress over the years in the design of bionic signals based on cetacean sounds. Some researchers use original cetacean sounds to construct bionic signals [11]. However, the original cetacean sound database is usually limited, and it is difficult to find original cetacean sounds that can meet the validity requirements of covert ASD and UAC. Due to this limitation, some researchers try to build suitable bionic signal models to mimic the original cetacean sounds [12]–[16], [24], [25].

Tonal sounds are a large and important subset of cetacean sounds, and they are produced by both toothed whales [26]–[28] and baleen whales [29], which are sister clades containing all extant whales. Although within cetaceans the acoustic characteristics of tonal sounds vary enormously, such sounds are broadly defined as frequency modulation (FM) signals [30], [31]. Furthermore, cetacean tonal sounds are usually characterized in terms of their time-frequency spectrograms (TFSs), which is usually referred to as the ''contour'' of a tonal sound [32].

Due to the wide distribution of tonal sounds as well as their diverse acoustic characteristics in terms of duration, frequency distribution and TF distribution, etc., the bionic signal models based on tonal sounds can meet different camouflage ability and validity requirements of covert ASD and UAC.

In order to meet the validity requirements, the bionic signal models should parameterize the tonal sounds, so that the parameters of the bionic signals can be conveniently adjusted according to the validity requirements of ASD and UAC. For the camouflage ability requirements, the bionic signal models should achieve high-similarity mimicry of various tonal sounds.

Conventional bionic signal models about tonal sounds can be mainly divided into two categories [12]–[16], [24], [25].

The first category [12], [24] is to use weighted signal superposition technology to synthesize bionic signals. The tonal sound is modeled as weighted superposition of harmonically related sinusoids, and single sinusoidal frequencies are estimated over the windowed data. Since the bionic signal is expressed as a signal consisting of a large amount of short data blocks, the ASD and UAC performance of the bionic signal can only be changed by modifying each data block, which is not practical.

The second category [13]–[16], [25] is to construct the bionic signal based on basic FM signal models. Chris Capus *et al.* proposed a bionic sonar signal model with a double down-chirp structure for bottlenose dolphin clicks [25], and obtained a high-similarity performance for bottlenose dolphin clicks with the double down-chirp structure. Ahmad E. *et al.* modeled dolphin whistles based on the basic FM signal model, such as linear frequency modulation (LFM) signal and hyperbolic frequency modulation (HFM) signal, and designed bionic signals carrying information bits for UAC [13], [14]. Liu *et al.* proposed to use a series of segmented LFM signals carrying digital information to mimic nonlinear frequency modulation (NFM) whistles to achieve bionic covert UAC [15]. In 2018, a bionic sonar signal model was proposed based on the HFM signal model, which realized the high similarity mimicry of false killer whale whistles and high-precision ASD [16]. Since the TF structures of these models are simple, it's difficult to achieve high-similarity imitation of cetacean sounds with complex NFM characteristics using these models.

In this paper, we propose two bionic signal models and one piecewise construction strategy for complex cetacean tonal sounds for covert ASD and UAC. By analyzing the contours of cetacean tonal sounds, it is found that the contours of cetacean sounds are similar to those of the power frequency modulation (PFM) signal and the sinusoidal frequency modulation (SFM) signal. Therefore, based on PFM and SFM signal models, two bionic signal models are presented, which can parameterize the characteristics, such as curvature, slope, frequency range and duration, of the tonal sound contours. Then, combined with the waveform envelope extraction method for time-domain signal and the piecewise construction strategy, high-similarity mimicry of various cetacean sounds is realized.

The main contributions of this paper can be summarized as follows:

(1) Two bionic signal models and their piecewise construction strategy are proposed, which realize the high-similarity mimicry of most cetacean tonal sounds and some cetacean sounds with simple or complex TF structures.

(2) The proposed method parameterizes the acoustic characteristics of cetacean sounds, so that the parameters of the synthesized bionic signals can be felicitously modified to obtain high camouflage ability and good detection and communication performance.

(3) The proposed method can construct bionic signals, whose characteristics are similar to those of existing

cetacean sounds. As a result, these constructed bionic signals can be applied to expand the existing cetacean sound database, and evaluate the behaviour impact of different acoustic characteristics on cetaceans.

II. PREPROCESSING AND ANALYSIS OF CETACEAN TONAL SOUNDS

In this paper, the tonal sounds of three common cetacean species, bottlenose dolphin, long-finned pilot whale and false killer whale, are taken as examples to illustrate the proposed models and method. The original high-quality cetacean tonal sounds were recorded with a 44.1ksps sampling rate. Considering that the tonal sounds were polluted by the Gaussian ocean ambient noise [33], a Wiener filter is utilized to remove the background noise of the recorded sounds, and the first 0.25 seconds of each original cetacean sound recording is utilized for a priori SNR estimation. By using the short-time Fourier transform (STFT) with a 1024-point (25ms) Hamming window with 60% overlap, the TFSs of the denoised tonal sounds are generated.

Tonal sounds are usually classified according to their contours [26]–[29], and due to the complexity and diversity of tonal species and sounds, a definition of the categories of tonal sound contours is usually specific for a certain cetacean species.

By studying various classification methods for tonal sounds, it is found that the classification method proposed by Bazúa-Durán and Au [26] has strong versatility, and could be applied to most tonal sounds. By using this classification method as a reference, most tonal sounds can be ascribed to one of the six categories according to their contours, as described in Table 1 and illustrated in Fig. 1, including constant frequency, upsweep, downsweep, concave, convex and sine.

TABLE 1. Description of six categories of tonal sounds.

Category	Description
Constant frequency	Frequency essentially remains constant throughout the entire duration of the tonal sound.
Upsweep	Frequency mainly ascends throughout all or most of the tonal sound.
Downsweep	Frequency mainly descends throughout all or most of the tonal sound.
Concave	Frequency mainly descends and then mainly ascends.
Convex	Frequency mainly ascends and then mainly descends.
Sine	Frequency mainly ascends, then mainly descends, and so forth, or vice versa.

As shown in Fig. 1, the constant frequency tonal sound essentially has no change in frequency, which is similar to continuous wave (CW) signal. In contrast, the five categories of upsweep, downsweep, concave, convex and sine tonal sounds are different from each other, and they all have complex NFM characteristics. Therefore, in order to ensure camouflage of the bionic signals, the bionic signal models should match the NFM characteristics of different tonal sounds.

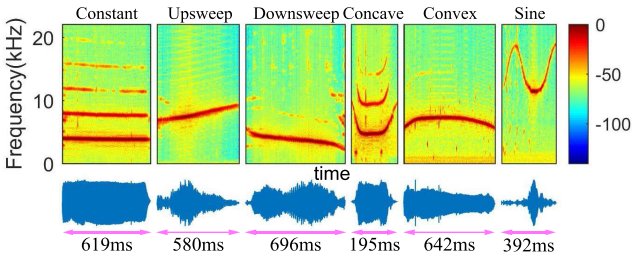

FIGURE 1. TFSs and waveforms of six categories of tonal sounds.

Furthermore, as can be seen from Fig. 1, the NFM characteristics of different parts of a tonal sound may be different, and these characteristics can be divided into two categories: the first category is that the absolute value of the contour slope changes monotonically, such as monotonically increasing, which is similar to the PFM signal; the second category is that the absolute value of the contour slope firstly increases and then decreases, which is similar to the SFM signal. Therefore, in the next section, based on the PFM signal model and the SFM signal model, we propose two bionic signal models, and use multiple bionic signals with different NFM characteristics to construct different parts of a tonal sound.

III. BIONIC SIGNAL MODELS

As the idea in this paper is to mimic cetacean tonal sounds from the perspective of contour characteristics, the first step is to construct the TF expression of bionic signal based on the tonal sound contour, and the last step is to transform the TF expression into the time-domain waveform. If the TF expression of a FM signal $s(t)$ is defined as $f(t)$, the corresponding phase function $\phi(t)$ can be defied as

$$\phi(t) = 2\pi \int_0^t f(\omega) d\omega. \tag{1}$$

Then, the FM signal $s(t)$ can be expressed as

$$s(t) = A(t) \cos[\phi(t)], \quad 0 \le t \le T, \tag{2}$$

where T is the duration and $A(t)$ denotes the signal envelope function.

A. POWER FREQUENCY MODULATION BIONIC (PFMB) SIGNAL MODEL

The first method of constructing the bionic signal model is based on the PFM signal model. A PFM signal [34] with duration T is defined as

$$\bar{s}_P(t) = A(t) \sin\left\{2\pi\left(\frac{Bt^{\alpha+1}}{(\alpha+1)T^{\alpha}} + f_C t\right)\right\}, \quad 0 \le t \le T, \tag{3}$$

where B is the bandwidth, f_C plays the part of the carrier frequency, and α ($\alpha > 0$) is a curvature adjustment factor. The instantaneous frequency of the PFM signal is expressed as

$$\bar{f}_P(t) = \frac{\partial}{\partial t}\left[\frac{Bt^{\alpha+1}}{(\alpha+1)T^{\alpha}} + f_C t\right] = B\left(\frac{t}{T}\right)^{\alpha} + f_C. \tag{4}$$

Furthermore, the contour slope of the PFM signal is

$$\bar{f}'_P(t) = \frac{\partial}{\partial t}\left[B\left(\frac{t}{T}\right)^{\alpha} + f_C\right] = \frac{B\alpha}{T}\left(\frac{t}{T}\right)^{\alpha-1}. \quad (5)$$

Obviously, $\bar{f}_P(t)$ is a power function of time t. The start frequency $\bar{f}_P(0)$ and the end frequency $\bar{f}_P(T)$ are f_C and $f_C + B$, respectively. Clearly, the contour curvature and contour slope of the SFM signal depends on its frequency range, duration and parameter α.

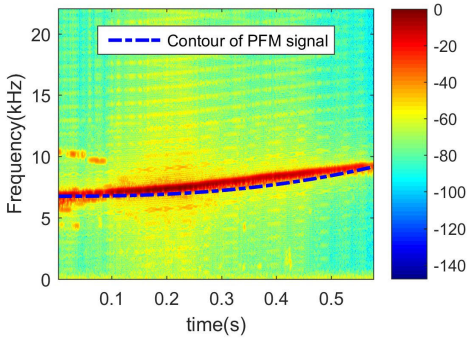

FIGURE 2. Contours of the upsweep tonal sound and the PFM signal.

However, when trying to fit the contour of an upsweep tonal sound using a PFM signal with $\alpha > 1$, we find that there is a significant mismatch between them, as shown in Fig. 2. This mismatch is caused by the different contour slope between the upsweep tonal sound and the PFM signal at time $t = 0$. As can be seen form (5), when $\alpha > 1$, the contour slope of the PFM signal at time $t = 0$ is always $\bar{f}'_P(0) = 0$, no matter how its frequency range, duration and parameter α change.

For a close match between the bionic signals and the tonal sounds, based on (4), the instantaneous frequency of a novel PFMB signal model is proposed as follows

$$f_P(t) = (B - kT)\left(\frac{t}{T}\right)^{\alpha} + kt + f_C, \quad 0 \le t \le T, \quad (6)$$

where the curvature adjustment factor α ($\alpha > 0$) is used to adjust the curvature of $f_P(t)$, and the slope adjustment factor k ($0 \le k \le B/T$) is used to adjust the slope of $f_P(t)$ at time $t = 0$ and $t = T$. Clearly, $f_P(t)$ continuously and monotonically goes from the start frequency $f_P(0) = f_C$ to the end frequency $f_P(T) = f_C + B$ within a signal duration in the way of PFM.

By substituting (6) into (1) and (2), we can obtain the corresponding PFMB signal model as follows

$$s_P(t) = A(t)\cos\left\{2\pi\left[\frac{(B - kT)\,t^{\alpha+1}}{(\alpha+1)\,T^{\alpha}} + \frac{1}{2}kt^2 + f_C t\right]\right\}, \quad (7)$$

As can be seen from (6) and (7), the PFMB signal model is more general than the PFM model. More specifically, when $k = 0$, $s_P(t)$ is equivalent to the PFM signal model; when $k = B/T$, $f_P(t) = Bt/T + f_C$ and $s_P(t)$ is equivalent to a LFM signal model. Specially, when $B = 0$, $f_P(t) = f_C$ and $s_P(t)$ is equivalent to a CW signal model.

The contour slope of $s_P(t)$ is defined as

$$f'_P(t) = \frac{\partial}{\partial t}\left[(B - kT)\left(\frac{t}{T}\right)^{\alpha} + kt + f_C\right] = \frac{(B - kT)\,\alpha t^{\alpha-1}}{T^{\alpha}} + k. \quad (8)$$

As can be seen form (6) and (8), due to the introduction of the slope adjustment factor k, the contour slope of $s_P(t)$ now depends on its frequency range, duration, curvature adjustment factor α and slope adjustment factor k. When the frequency range and duration of $s_P(t)$ are fixed, the contour curvature can be adjusted by changing the parameter α, and the contour slope at time $t = 0$ and $t = T$ can be adjusted by changing the parameter k, which is very important to mimic the contours of true tonal sounds as closely as possible.

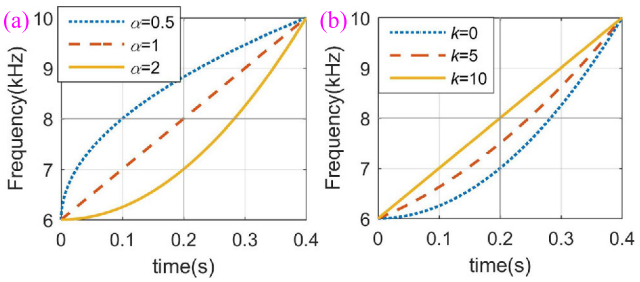

FIGURE 3. (a) The contours of PFMB signals $s_P(t)$ with three different curvature adjustment factors α. (b) The contours of PFMB signals $s_P(t)$ with three different slope adjustment factors k.

For example, when carrier frequency $f_C = 6$kHz, bandwidth $B = 4$kHz, duration $T = 0.4$s, and half of the frequency range is $f_{1/2} = f_C + B/2 = 8$kHz, the contours of $s_P(t)$ with different curvature adjustment factors α and slope adjustment factors k are shown in Fig. 3(a) and Fig. 3(b), respectively. When the parameter k is constant ($k = 0$), the contours of $s_P(t)$ with three different parameters α are shown in Fig. 3(a). Besides, when the parameter α is constant ($\alpha = 2$), the contours of $s_P(t)$ with three different parameters k are shown in Fig. 3(b).

As shown in Fig. 3(a), with the change of α, the contour curvature of $s_P(t)$ changes, and the value of α also affects the monotonicity of the contour slope $f'_P(t)$ and the varying speed of $f_P(t)$. When $0 < \alpha < 1$, the contour slope $f'_P(t)$ decreases monotonically with time t, and therefore, $f_P(t)$ changes faster in the frequency range below $f_{1/2}$ and $f_P(T/2) > f_{1/2}$; for $\alpha = 1$, $f'_P(t)$ is always B/T, which means $s_P(t)$ is equivalent to a LFM signal and $f_P(T/2)$ is exactly $f_{1/2}$; when $\alpha > 1$, $f'_P(t)$ increases monotonically with t, and therefore, $f_P(t)$ changes faster in the frequency range above $f_{1/2}$ and $f_P(T/2) < f_{1/2}$.

It can be seen from Fig. 3(b) that as k increases from 0 to $B/T = 10$, the contour slope of $s_P(t)$ at time $t = 0$ and $t = T$ also changes continuously and gradually approaches B/T.

Therefore, one can mimic the contours of the true tonal sounds as closely as possible by adjusting α and k on the condition that the frequency range and the duration are fixed.

B. SINUSOIDAL FREQUENCY MODULATION BIONIC (SFMB) SIGNAL MODEL

The second method of constructing the bionic signal model is based on the SFM signal model. A SFM signal [35] with a duration T is defined as

$$\bar{s}_S(t) = A(t)\cos\left\{2\pi\left[-\frac{TB}{2\pi}\sin\frac{\pi t}{T}+\left(f_C+\frac{B}{2}\right)t\right]\right\}, \quad 0\le t\le T. \tag{9}$$

The instantaneous frequency of the SFM signal is

$$\bar{f}_S(t) = -\frac{B}{2}\cos\frac{\pi t}{T}+\frac{B}{2}+f_C. \tag{10}$$

Furthermore, the contour slope of the SFM signal is

$$\bar{f}'_S(t) = \frac{\partial}{\partial t}\left[\frac{B}{2}\cos\left(\frac{\pi t}{T}+\pi\right)+\frac{B}{2}+f_C\right] = -\frac{B\pi}{2T}\sin\left(\frac{\pi t}{2T}\right). \tag{11}$$

Obviously, $\bar{f}_S(t)$ is a sinusoidal function of time t. The start frequency $\bar{f}_S(0)$ and the end frequency $\bar{f}_S(T)$ are f_C and f_C+B, respectively. Clearly, the contour curvature and contour slope of the SFM signal only depends on its frequency range and duration.

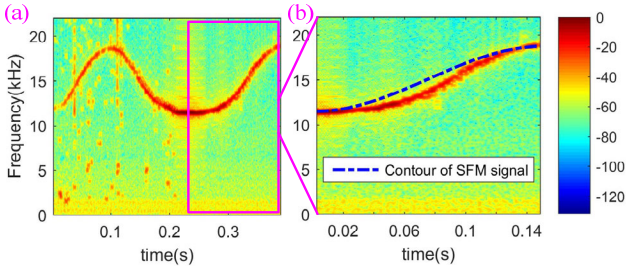

FIGURE 4. Contours of sine tonal sound and the SFM signal.

However, when trying to fit a part of the contour of a sine tonal sound using the SFM signal, we find that there is a significant mismatch between them. Fig. 4(a) shows the complete contour of a sine tonal sound, the contours of a SFM signal and part of the sine tonal sound are shown in Fig. 4(b). This mismatch is caused by the different contour curvatures between the tonal sound and the SFM signal. As can be seen from (10), once the frequency range and the duration of a SFM signal are fixed, neither its contour curvature nor its slope can be changed.

To have a close match to the true tonal sounds, based on (10), and referring to the method of changing the contour curvature and contour slope in the PFMB signal model, the instantaneous frequency of a novel SFMB signal model is proposed as follows

$$f_S(t) = (B-hT)\sin^\beta\left(\frac{\pi t}{2T}\right)+ht+f_C, \tag{12}$$

where the curvature adjustment factor β ($\beta>0$) is used to adjust the curvature of $f_S(t)$, the slope adjustment factor k ($0\le k\le B/T$) is used to adjust the slope of $f_P(t)$ at time $t=0$ and $t=T$. Clearly, $f_P(t)$ continuously and monotonically changes from the start frequency $f_P(0)=f_C$ to the end frequency $f_P(T)=f_C+B$ within a signal duration as in SFM.

By substituting (12) into (1) and (2), we can obtain the corresponding SFMB signal model as follows

$$s_S(t) = A(t)\cos\left[2\pi\int_0^t f_S(\omega)d\omega\right] = A(t)\cos\left\{2\pi\int_0^t\left[(B-hT)\sin^\beta\left(\frac{\pi\omega}{2T}\right)+h\omega+f_C\right]d\omega\right\}. \tag{13}$$

As can be observed from (12) and (13), the proposed SFMB signal model is more general compared to the SFM signal model. More specifically, when $h=0$ and $\beta=2$, $s_S(t)$ is equivalent to the SFM signal model; for $h=B/T$, $f_S(t)=Bt/T+f_C$ and $s_S(t)$ is equivalent to an LFM signal model. Specially, when $B=0$, $f_P(t)=f_C$ and $s_S(t)$ is equivalent to a CW signal.

Most importantly, the contour slope of $s_S(t)$ is

$$f'_S(t) = \frac{\partial}{\partial t}\left[(B-hT)\sin^\beta\left(\frac{\pi t}{2T}\right)+ht+f_C\right] = (B-hT)\frac{\beta\pi}{2T}\sin^{\beta-1}\left(\frac{\pi t}{2T}\right)\cos\left(\frac{\pi t}{2T}\right)+h. \tag{14}$$

As can be seen from (12) and (14), due to the addition of the curvature adjustment factor β and the slope adjustment factor h, the contour curvature and contour slope of $s_S(t)$ now depend on its frequency range, duration, parameter h and parameter β. When the frequency range and duration of $s_S(t)$ are fixed, the contour curvature can be adjusted by changing β, and the contour slope at time $t=0$ and $t=T$ can be adjusted by changing k, which is very important for us to mimic the contours of the true tonal sounds as closely as possible.

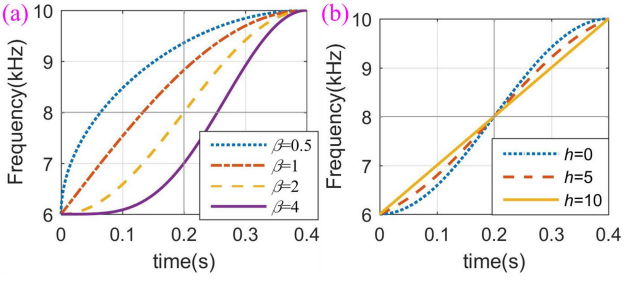

FIGURE 5. (a) The contours of SFMB signals $s_S(t)$ with four different curvature adjustment values of β. (b) The contours of SFMB signals $s_S(t)$ with three different slope adjustment values of h.

For example, when bandwidth $B=4$kHz, carrier frequency $f_C=6$kHz, and duration $T=0.4$s, the contours of $s_S(t)$ with different curvature adjustment factors β and slope adjustment factors h are shown in Fig. 5. When the parameter h is constant ($h=0$), the contours of $s_S(t)$ with four different values of β are shown in Fig. 5(a). Besides, when β is constant

($\beta = 2$), the contours of $s_P(t)$ with three different values of h are shown in Fig. 5(b).

It can be seen from Fig. 5(a) that with the change of β, the contour curvature of $s_P(t)$ also changes. Besides, the monotonicity of $f_S'(t)$ and the varying speed of $f_P(t)$ are also affected by the value range of β; when $0 < \beta \leq 1$, $f_S'(t)$ decreases monotonically as time t increases; when $\beta > 1$, $f_S'(t)$ increases first and then decreases as time t increases. Furthermore, the value range of β also affects the varying speed of $f_P(t)$, when $0 < \beta < 2$, $f_S(t)$ varies faster in the frequency range below $f_{1/2}$ and therefore $f_S(T/2) > f_{1/2}$; for $\beta = 2$, $f_S(t)$ is symmetric about the center point $(T/2, f_{1/2})$ and thus $f_S(T/2) = f_{1/2}$; when $\beta > 2$, $f_P(t)$ varies slower in the frequency range below $f_{1/2}$, so that $f_P(T/2) < f_{1/2}$.

As shown in Fig. 5(b), the contour slope of $s_S(t)$ at time $t = 0$ and $t = T$ changes continuously and gradually approaches B/T as h increases from 0 to $B/T = 10$.

Therefore, one can mimic the contours of the true tonal sounds as closely as possible by adjusting β and h on the condition that the frequency range and the duration are fixed.

Moreover, by comparing Fig. 3(a) and Fig. 5(a), it can be observed that when $\alpha < 1$ and $\beta < 1$, both contour slopes of the PFMB signal ($f_P'(t)$) and the SFMB signal ($f_S'(t)$) change monotonically. When $k = 0$ and $h = 0$, $f_P'(t)$ with four different values of α are shown in Fig. 6(a), and $f_S'(t)$ with four different values of β are shown in Fig. 6(b). It can be observed that $f_P'(T)$ is always greater than zero, whereas $f_S'(T)$ is always zero when $t = T$.

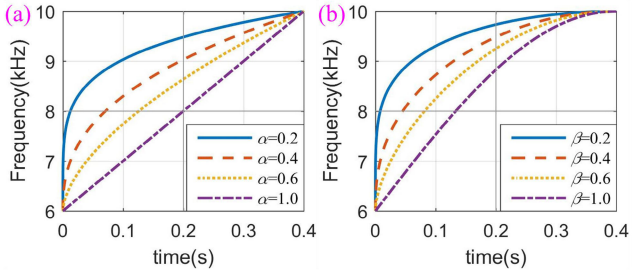

FIGURE 6. (a) The contours of PFMB signals $s_P(t)$ with four different curvature adjustment values of α. (b) The contours of SFMB signals $s_S(t)$ with four different curvature adjustment values of β.

From (8), it can be demonstrated that $f_P'(T) = \alpha(B/T - k) + k$, since $\alpha > 0$ and $0 \leq k \leq B/T$, no matter how α and k change, $f_P'(T) > 0$ always holds, which means the contour slope of the PFMB signal $s_P(t)$ is always greater than 0 at time $t = T$. However, from (14), it can be demonstrated that $f_S'(T) = h$, which means that the contour slope of the SFMB signal $s_S(t)$ is determined only by h, and $f_S'(T) = 0$ always holds when $h = 0$.

C. SUB BIONIC SIGNAL MODELS

As analyzed above, PFMB and SFMB signal models can only be utilized to match tonal sounds with monotonically increasing frequency.

In order to increase the diversity of bionic signals based on the PFMB signal model and the SFMB signal model, we propose four corresponding sub-signal models.

Based on the TF expression of the PFMB signal model defined by (6), four sub-PFMB TF expressions $f_{PO}(t)$, $f_{PX}(t)$, $f_{PY}(t)$ and $f_{PZ}(t)$ are defined as follows

$$f_{PO}(t) = f_P(t) = (B - kT)\left(\frac{t}{T}\right)^{\alpha} + kt + f_C, \tag{15}$$

$$f_{PX}(t) = -f_P(t) + B + 2f_C = (kT - B)\left(\frac{t}{T}\right)^{\alpha} - kt + B + f_C, \tag{16}$$

$$f_{PY}(t) = f_P[-(t - T)] = (B - kT)\left(1 - \frac{t}{T}\right)^{\alpha} - k(t - T) + f_C, \tag{17}$$

$$f_{PZ}(t) = -f_P[-(t - T)] + B + 2f_C = (kT - B)\left(1 - \frac{t}{T}\right)^{\alpha} + k(t - T) + B + f_C. \tag{18}$$

Through (1) and (2), we can obtain four sub-PFMB signal models $s_{PO}(t)$, $s_{PX}(t)$, $s_{PY}(t)$ and $s_{PZ}(t)$.

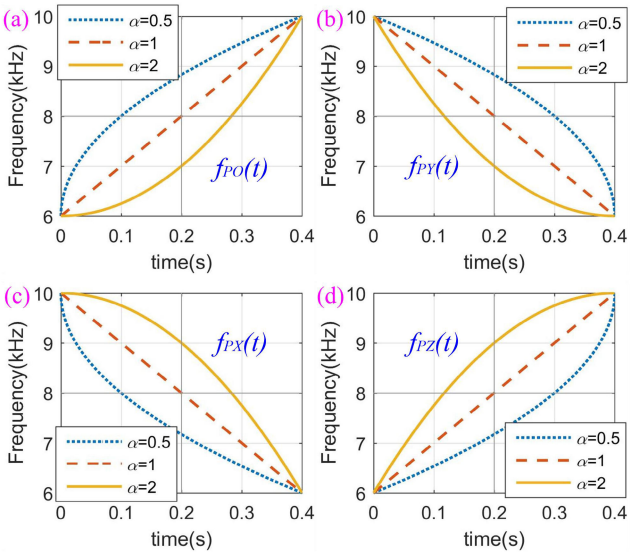

FIGURE 7. (a)-(d) The curves with three different curvature adjustment values of α for $f_{PO}(t)$, $f_{PY}(t)$, $f_{PX}(t)$and $f_{PZ}(t)$, respectively.

Obviously, $f_{PO}(t)$, $f_{PX}(t)$, $f_{PY}(t)$ and $f_{PZ}(t)$ are power functions of time t. When the frequency range is 6 to 10 kHz and the duration $T = 0.4$s, the curves of these TF expressions with three different α parameters are shown in Fig. 7(a)-(d). It can be seen that $f_{PO}(t)$ is identical to the TF expression of the original PFMB signal model $f_P(t)$, and $f_{PO}(t)$ is symmetric with $f_{PX}(t)$, $f_{PY}(t)$ and $f_{PZ}(t)$ about the axis $f_{PO}(t) = B/2 + f_C$, axis $t = T/2$ and center point $(T/2, B/2 + f_C)$, respectively. Besides, $f_{PO}(t)$ and $f_{PZ}(t)$ changes from the start frequency f_C to the end frequency $B + f_C$ within a signal duration T, whereas $f_{PX}(t)$ and $f_{PY}(t)$ goes from the start frequency $B + f_C$ to the end frequency f_C within the same duration T.

In a similar way, based on the TF expression of the SFMB signal model defined by (12), four sub-SFMB TF expressions $f_{SO}(t), f_{SX}(t), f_{SY}(t)$ and $f_{SZ}(t)$ are defined as follows

$$\begin{aligned} f_{SO}(t) &= f_S(t) \\ &= (B - hT)\sin^{\beta}\left(\frac{\pi t}{2T}\right) + ht + f_C, \end{aligned} \tag{19}$$

$$\begin{aligned} f_{SX}(t) &= -f_S(t) + B + 2f_C \\ &= (hT - B)\sin^{\beta}\left(\frac{\pi t}{2T}\right) - ht + B + f_C, \end{aligned} \tag{20}$$

$$\begin{aligned} f_{SY}(t) &= f_S[-(t-T)] \\ &= (B - hT)\sin^{\beta}\left[\frac{\pi(-t+T)}{2T}\right] \\ &\quad + h(-t+T) + f_C, \end{aligned} \tag{21}$$

$$\begin{aligned} f_{SZ}(t) &= -f_S[-(t-T)] + B + 2f_C \\ &= (hT - B)\sin^{\beta}\left[\frac{\pi(-t+T)}{2T}\right] \\ &\quad + h(t-T) + B + f_C. \end{aligned} \tag{22}$$

Through (1) and (2), we can obtain four sub-SFMB signal models $s_{SO}(t)$, $s_{SX}(t)$, $s_{SY}(t)$, $s_{SZ}(t)$.

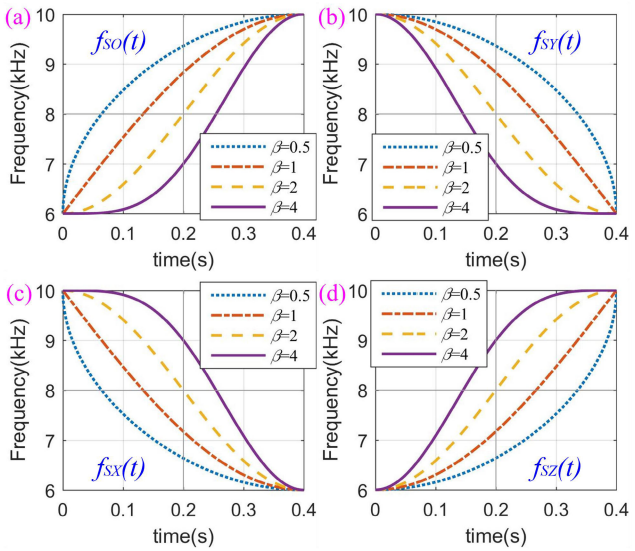

FIGURE 8. (a)-(d) The curves with four different curvature adjustment values of β for $f_{SO}(t)$, $f_{SY}(t)$, $f_{SX}(t)$and $f_{SZ}(t)$, respectively.

Obviously, $f_{SO}(t), f_{SX}(t), f_{SY}(t)$ and $f_{SZ}(t)$ are sinusoidal functions of time t, and $f_{SO}(t)$ is identical to the TF expression of the original SFMB signal model $f_S(t)$. When the frequency range is 6 to 10 kHz and the duration $T = 0.4$s, the curves of $f_{SO}(t), f_{SY}(t), f_{SX}(t)$ and $f_{SZ}(t)$ with four different β parameters are shown in Fig. 8(a)-(d), respectively. It can be seen that f_{SO} is symmetric with $f_{SX}(t)$, $f_{SY}(t)$ and $f_{SZ}(t)$ about the axis $f_{SO}(t) = B/2 + f_C$, axis $t = T/2$ and center point $(T/2, B/2 + f_C)$, respectively. Besides, for $f_{SO}(t)$ and $f_{SZ}(t)$, the start frequency and end frequency are f_C and $B+f_C$, respectively, whereas those of $f_{SX}(t)$ and $f_{SY}(t)$ are $B + f_C$ and f_C, respectively.

D. PIECEWISE CONSTRUCTION STRATEGY FOR COMPLEX TONAL SOUNDS

For a tonal sound with a simple contour, a sub-PFMB signal or a sub-SFMB signal is sufficient for accurate mimicry. However, in reality, the contours of most tonal sounds are complex, and as can be observed from Fig. 4, a bionic signal can only match a part of a tonal sound. In this case, a piecewise construction strategy for complex tonal sounds is proposed.

Suppose that the bionic signal corresponding to a tonal sound is expressed as $s_B(t)$. To construct $s_B(t)$, the tonal sound is first divided into M segments. In order to reduce the complexity of constructing bionic signals, under the condition of ensuring similarity between the bionic signal contour and the tonal sound contour, M should be as small as possible. Then, M bionic signal segments are constructed to mimic M segments of the tonal sound. Finally, by putting these M bionic signal segments together in the time domain, we can obtain $s_B(t)$. Fig. 9 shows the piecewise construction strategy for the complex tonal sounds.

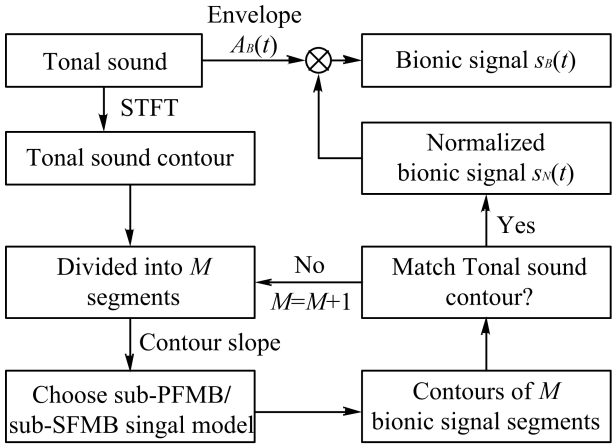

FIGURE 9. Piecewise construction strategy for complex tonal sounds.

As shown in Fig. 9, the bionic signal $s_B(t)$ consisting of M bionic signal segments is expressed as

$$s_B(t) = A_B(t) \cdot s_N(t) \tag{23}$$

where $A_B(t)$ is the envelope of $s_B(t)$, $s_N(t)$ is the normalized bionic signal, which is $s_B(t)$ before amplitude modulation and expressed as

$$\begin{aligned} s_N(t) = s_{B,1}\left(t - T_{D,1}\right) + \cdots + s_{B,m}\left(t - T_{D,m}\right) \\ + \cdots s_{B,M}\left(t - T_{D,M}\right), \end{aligned} \tag{24}$$

where $s_{B,m}(t)$ is the mth bionic signal segment of $s_B(t)$, $m = 1, 2, \cdots, M$. The duration of $s_{B,m}(t)$ is $T_{B,m}$, and the time delay $T_{D,m}$ denotes the total duration of all bionic signal segments in the signal set $\{s_{B,1}(t), \cdots, s_{B,m-1}(t)\}$ with

$$T_{D,m} = T_{B,m-1} + \cdots + T_{B,1}. \tag{25}$$

In general, the time delay for the first bionic signal segment $s_{B,1}(t)$ is $T_{D,1} = 0$, which means $s_{B,1}\left(t - T_{D,1}\right) = s_{B,1}(t)$.

More specifically, the piecewise construction strategy can be divided into the following four steps:

Step 1: Design the TF expression of each bionic signal segment $s_{B,m}(t)$.

For each bionic signal segment, choosing sub-PFMB signal models or sub-SFMB models is based on the contour slope of each tonal sound segment. If the absolute value of the contour slope changes monotonically, both sub-PFMB signal models and sub-SFMB models are suitable. However, when the absolute value of the contour slope firstly increases and then decreases, only sub-SFMB signal models are appropriate.

Furthermore, the TF expression of each bionic signal segment is designed by changing the parameters of the bionic signal model, including curvature adjustment factor α (or β), slope adjustment factor k (or h), duration T, carrier frequency f_C and bandwidth B.

In order to ensure a high similarity between the bionic signal and the original tonal sound, the smoothness of the contour of the bionic signal should be consistent with that the tonal sound; if the contour of the original tonal changes continuously, the frequency and contour slope should change continuously where two adjacent bionic signal segments are connected. For example, if a bionic signal consists of two bionic signal segments $s_{B,1}(t)$ $(0 \le t \le T_{B,1})$ and $s_{B,2}(t)$ $(0 \le t \le T_{B,2})$, and their TF expressions are $f_{B,1}(t)$ and $f_{B,2}(t)$, respectively, to ensure a smooth transition between $f_{B,1}(t)$ and $f_{B,1}(t)$, the following two conditions should be satisfied:

$$f_{B,1}\left(T_{B,1}\right) = f_{B,1}(0), \tag{26}$$

$$\left.\frac{\partial f_{B,1}(t)}{\partial t}\right|_{t=T_{B,1}} = \left.\frac{\partial f_{B,2}(t)}{\partial t}\right|_{t=0}. \tag{27}$$

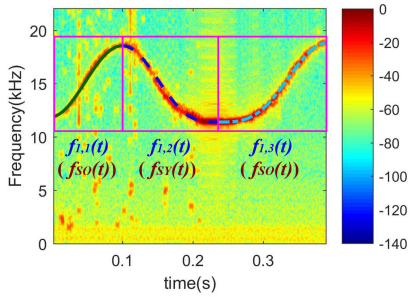

FIGURE 10. Contours of the sine tonal sound and three bionic signal segments.

For example, as shown in Fig. 10, the contour of the sine tonal sound in Fig. 4 can be mimicked by three bionic signal segments $s_{B,1}(t)$, $s_{B,2}(t)$ and $s_{B,3}(t)$. The contours of these three bionic signal segments are expressed as $f_{B,1}(t), f_{B,2}(t)$, and $f_{B,3}(t)$, respectively, and they are constructed based on $f_{SO}(t), f_{SY}(t)$, and $f_{SO}(t)$, respectively.

Step2: Construct the normalized bionic signal $s_N(t)$.

The mth bionic signal segment of the bionic signal $s_B(t)$ is defined as

$$\begin{aligned} s_{B,m}(t) &= \cos\left[\phi_{B,m}(t)\right] \\ &= \cos\left[2\pi \int_0^{T_{B,m}} f_{B,m}(t)dt\right], \quad 0 \le t \le T_{B,m}, \end{aligned} \tag{28}$$

where $\phi_{B,m}(t)$ is the phase function, and $f_{B,m}(t)$ is the TF expression of a sub-PFMB signal or a sub-SFMB signal.

Then, each bionic signal segment is shifted along the time axis, and the mth bionic signal segment $s_{B,m}(t)$ is shifted for $T_{D,m}$ and is expressed as

$$\begin{aligned} &s_{B,m}\left(t - T_{D,m}\right) \\ &\quad = \cos\left[\phi_{B,m}\left(t - T_{D,m}\right) + \Delta\phi_{B,m}\right], \\ &\quad T_{D,m} \le t \le T_{B,m} + T_{D,m}. \end{aligned} \tag{29}$$

Substituting M shifted bionic signal segments $s_{B,m}\left(t - T_{D,m}\right)$ into (24), we can obtain the waveform of $s_N(t)$.

It is noteworthy that $\Delta\phi_{B,m}$ is the phase compensation component, which is added to avoid the abrupt phase change between two adjacent bionic signal segments, and $\Delta\phi_{B,m}$ is defined as

$$\Delta\phi_{B,m} = \phi_{B,m-1}\left(T_{B,m-1}\right) + \cdots \phi_{B,1}\left(T_{B,1}\right). \tag{30}$$

Obviously, the phase compensation for the first bionic signal segment $s_{B,1}(t)$ is $\Delta\phi_{B,1} = 0$.

Therefore, by transforming the TF expressions $f_{B,1}(t)$, $f_{B,2}(t)$, and $f_{B,3}(t)$ in Fig. (8) into waveforms in the time domain, we can obtain the normalized bionic signal $s_N(t)$. The waveform and TFS of $s_N(t)$ are shown in Fig. 11 (a) and (b), respectively.

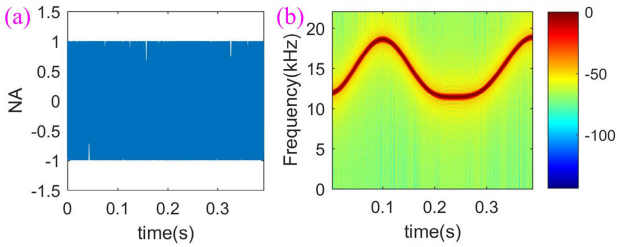

FIGURE 11. (a) The waveform of the normalized bionic signal $s_N(t)$. (b) TFS of the normalized bionic signal $s_N(t)$.

Step 3: Construct the envelope $A_B(t)$ of the bionic signal $s_B(t)$.

So far the signal envelope $A_B(t)$ has not been considered yet. It can be seen from Fig. 1 that different from the conventional ASD and UAC signal waveforms (such as CW, LFM, and HFM), the envelopes of the tonal sounds are not rectangular, and varies with different irregularity for different tonal sounds. Therefore, the envelope of each bionic signal $s_B(t)$ should be fit to that of the corresponding tonal sound. The envelope extraction method used here is based on the one proposed in [16].

Firstly, the STFT with a N-point Hamming window of the denoised tonal sounds is calculated. The denoised tonal sound is a discrete-time signal, expressed as

$$x[n] = a[n]\cos(\phi[n]), \tag{31}$$

where $a[n]$ and $\phi[n]$ are the envelope and phase of $x[n]$, respectively. The discrete STFT for $x[n]$ can be expressed as $X[k, l]$, where k is the block number and l is the frequency bin index. $X_k[l]$ is the discrete Fourier transform (DFT) for the kth block.

Secondly, obtain the envelope $a[n]$ from $X_k[l]$. If τ_k is the starting point of the kth block, then the amplitude of $x[n]$ at τ_k is $a[\tau_k] = A_k$. The peak value of $X_k[l]$ is expressed as $P_k = \max|X_k(l)|$. Since P_k is modulated by the Hamming window and DFT, a amplitude recovery factor is obtain by

$$K = \frac{1}{0.27N}. \tag{32}$$

Finally, let $a[\tau_k] = KP_k$ and the amplitude of $a[\tau_k]$ is restored to the same level as the tonal sound envelope. By using the piecewise cubic Hermit interpolation to add the remaining points of $a[n]$, the extracted envelope of $x[n]$ is obtained.

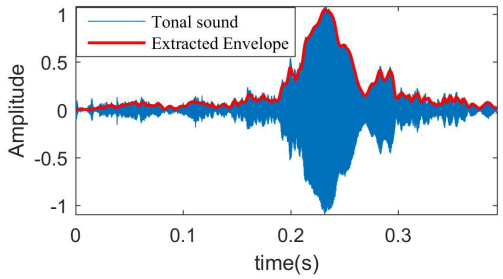

FIGURE 12. Waveform of the sine tonal sound and the corresponding extracted envelope.

The extracted envelope $a[n]$ and the waveform of the sine tonal sound are shown in Fig. 12, where it can be seen that $a[n]$ matches the envelope of the tonal sound well.

Step 4: Substituting the envelope $A_B(t)$ and the normalized bionic signal $s_N(t)$ into (23), we can obtain the bionic signal $s_B(t)$. The sine tonal sound and its TFS and the bionic signal $s_B(t)$ and its TFS are shown in Fig. 13. It can be seen that the bionic sonar signal can match the true whale whistles very well in terms of not only envelopes but also contours.

Besides, if a tonal sound has R harmonics, its corresponding bionic signal can be expressed as

$$s_B(t) = \sum_{r=1}^{R} s_r(t), \tag{33}$$

where $s_r(t)$ is the rth harmonic of $s_B(t)$, constructed according to the four steps above. Furthermore, the frequency of the rth harmonic $f_r(t)$ is designed to be integer multiples of the fundamental frequency $f_1(t)$, i.e.

$$f_r(t) = r \cdot f_1(t), \quad 2 \le r \le R. \tag{34}$$

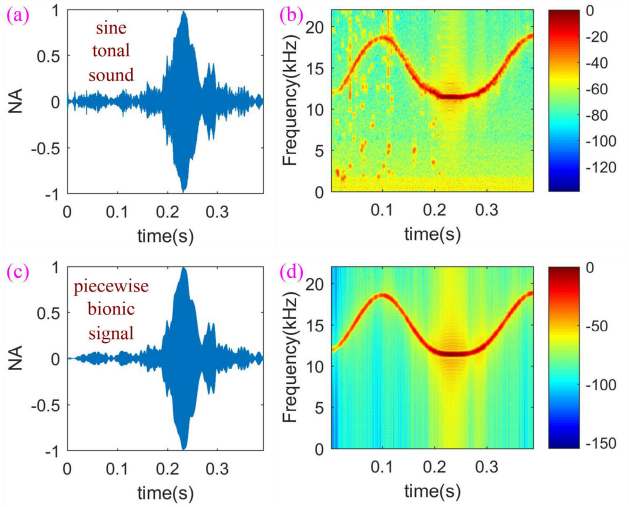

FIGURE 13. (a) The sine tonal sound. (b) The TFS of the sine tonal sound. (c) The bionic signal. (d) The TFS of the bionic signal.

IV. EXPERIMENTS AND RESULTS

A. SYNTHESIS OF SIX CATEGORIES OF TONAL SOUNDS

In this section, we examine the synthetic performance of the proposed method. Bionic signals corresponding to six categories of tonal sounds (constant frequency, upsweep, downsweep, concave, convex and sine) described in Table 1 are synthesized. Furthermore, one high-quality and representative of each category of tonal sounds are chosen to be matched and mimicked. The true tonal sounds and their TFSs and the constructed bionic signal waveforms and their TFSs are shown in Figs. 14-19. It can be seen that the constructed bionic signals have a close match to the true tonal sounds in terms of both envelopes and TFSs.

The waveforms and TFSs of the constant frequency tonal sounds T_cf1 and the corresponding bionic signals B_cf1 are shown in Fig. 14(a)-(d). Besides, the waveforms and TFSs of the constant frequency tonal sounds T_cf2 and the corresponding bionic signals B_cf2 are shown in Fig. 14(e)-(h).

The waveforms and TFSs of the upsweep tonal sounds T_up1 and the corresponding bionic signals B_up1 are shown in Fig. 15(a)-(d), and those of the upsweep tonal sounds T_up2 and the corresponding bionic signals B_up2 are shown in Fig. 15(e)-(h).

The waveforms and TFSs of the downsweep tonal sounds T_down1 and the corresponding bionic signals B_down1 are shown in Fig. 16(a)-(d), and those of the downsweep tonal sounds T_down2 and the corresponding bionic signals B_down2 are shown in Fig. 16(e)-(h).

The waveforms and TFSs of the concave tonal sounds T_concave1 and the corresponding bionic signals B_concave1 are shown in Fig. 17(a)-(d), and for the concave tonal sounds T_concave2 and the corresponding bionic signals B_concave2, they are shown in Fig. 17(e)-(h).

For the convex tonal sounds T_convex1 and T_convex2, and their corresponding bionic signals B_convex1 and

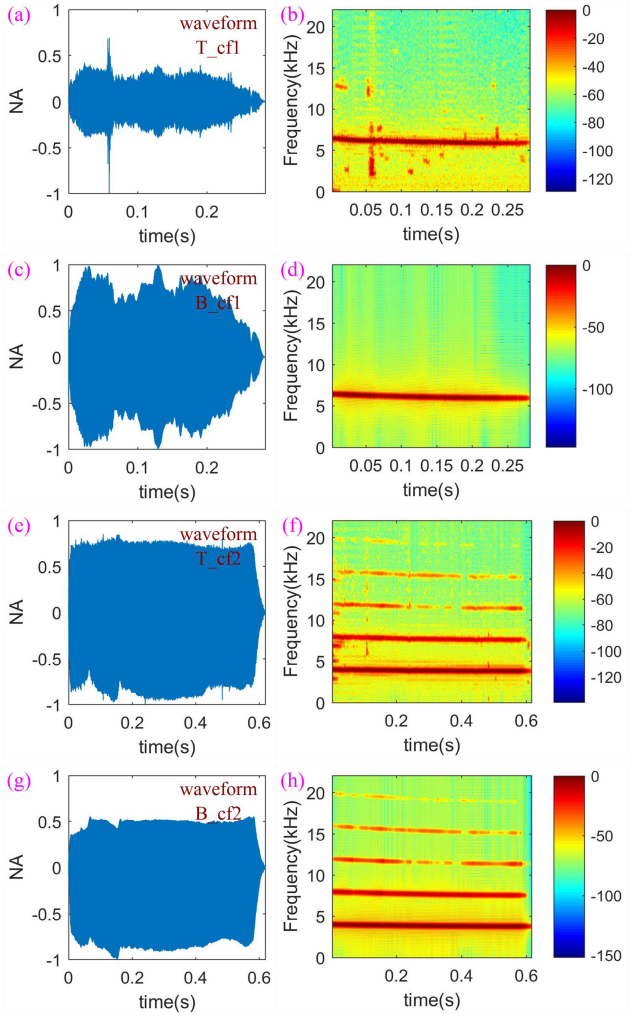

FIGURE 14. (a) The constant frequency tonal sounds T_cf1. (b) The TFS of T_cf1. (c) The bionic signal B_cf1. (d) The TFS of B_cf1. (e) The constant frequency tonal sounds T_cf2. (f) The TFS of T_cf2. (g) The bionic signal B_cf2. (h) The TFS of B_cf2.

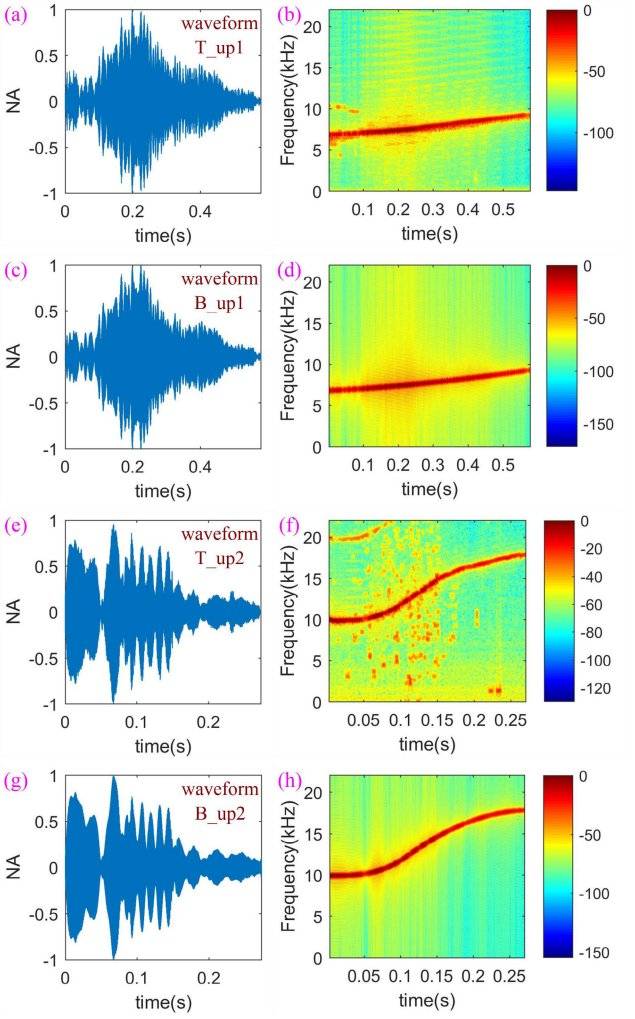

FIGURE 15. (a) The upsweep tonal sounds T_up1. (b) The TFS of T_up1. (c) The bionic signal B_up1. (d) The TFS of B_up1. (e) The upsweep tonal sounds T_up2. (f) The TFS of T_up2. (g) The bionic signal B_up2. (h) The TFS of B_up2.

B_convex2, the results are shown in Fig. 18(a)-(h), while for T_sine1 and T_sine2, and the corresponding bionic signals B_sine1 and B_sine2, they are shown in Fig. 19(a)-(h).

B. SYNTHESIS OF COMPLEX CETACEAN SOUNDS

In the second experiment, we examine the performance of the proposed method for synthesizing complex cetacean sounds.

In addition to tonal sounds, cetaceans can also produce some FM sounds with relatively long duration and complex TF structures, such as signature whistles [36]. Since these complex cetacean sounds can be divided into multiple simple FM signals, the proposed bionic signal models and the piecewise construction strategy can also be utilized to synthesize complex cetacean sounds.

An example is shown in Fig. 20, where 21 bionic signal segments are constructed to achieve high-similarity mimicry. The waveforms and TFSs of the complex cetacean sounds C_complex and B_complex are shown in Fig. 20(a)-(d). It can be seen that the constructed bionic signals can match the complex cetacean sounds very well.

C. CAMOUFLAGE ABILITY EVALUATION

In the third experiment, the camouflage ability of the constructed bionic signals is examined.

Since the contours of tonal sounds have obvious FM characteristics, and present acoustic classifiers usually classify a tonal sound based on its contour [26]–[29], the camouflage ability of a synthesized bionic signal depends on the similarity between its contour and that of the true tonal sound. The Pearson correlation coefficient (PCC), which is widely used in the measurement of the similarity between two data sets [37], is used to measure the similarity between the contours of the true tonal sounds and the synthesized bionic signals.

The extracted contour of a true tonal sound is $f_T[n] = \{f_{T\_1}, f_{T\_2}, \cdots, f_{T\_n}\}$, and the contour of the corresponding bionic signal is $f_B[n] = \{f_{B\_1}, f_{B\_2}, \cdots, f_{B\_n}\}$,

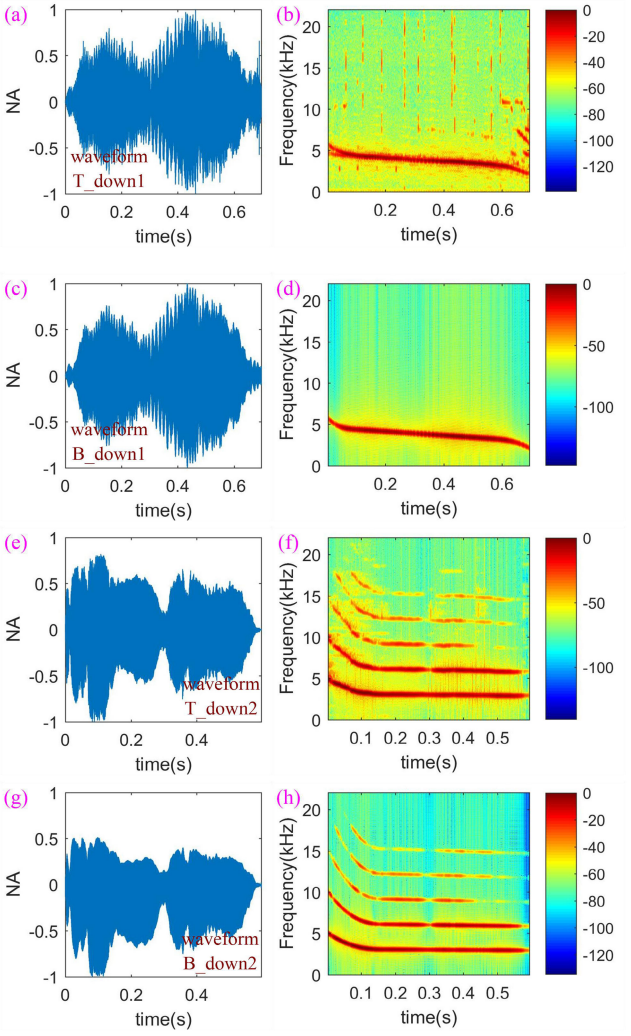

FIGURE 16. (a) The downsweep tonal sounds T_down1. (b) The TFS of T_down1. (c) The bionic signal B_down1. (d) The TFS of B_down1. (e) The downsweep tonal sounds T_down2. (f) The TFS of T_down2. (g) The bionic signal B_down2. (h) The TFS of B_down2.

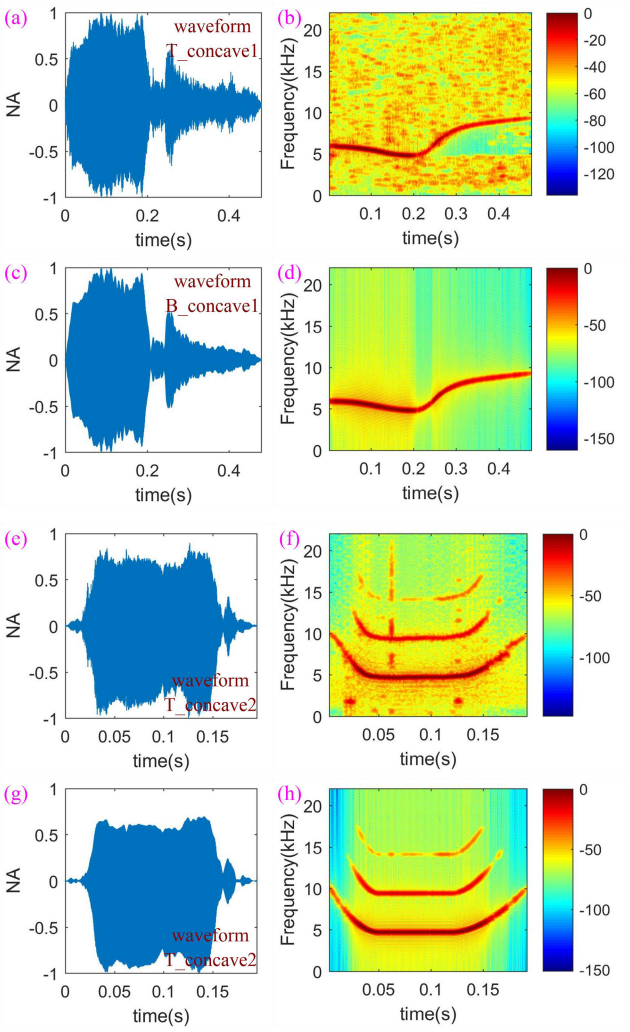

FIGURE 17. (a) The concave tonal sounds T_concave1. (b) The TFS of T_concave1. (c) The bionic signal B_concave1. (d) The TFS of B_concave1. (e) The concave tonal sounds T_concave2. (f) The TFS of T_concave2. (g) The bionic signal B_concave2. (h) The TFS of B_concave2.

where n is the data number of $f_T[n]$ and $f_B[n]$. Then, the PCC [37] between $f_T[n]$ and $f_B[n]$ is defined as

$$r_{TB} = \frac{\sum_{i=1}^{n}\left[\left(f_T - \bar{f}_T\right)\cdot\left(f_{B\_i} - \bar{f}_B\right)\right]}{\sqrt{\sum_{i=1}^{n}\left(f_{T\_i} - \bar{f}_T\right)^2 \cdot \sum_{i=1}^{n}\left(f_{B\_i} - \bar{f}_B\right)^2}}, \tag{35}$$

where $\bar{f}_T$ and $\bar{f}_B$ are the mean values of $f_T[n]$ and $f_B[n]$, respectively. The closer the r_{TB} is to 1, the higher the correlation between $f_T[n]$ and $f_B[n]$, that is, the better the camouflage ability of the bionic signal.

Table 2 shows the PCC between 13 true cetacean sounds and their corresponding bionic signals (shown in Figs. 14-20). It can be seen that all 13 PCC results are higher than 0.97, and 11 results of them are no less than 0.99, which means that the contours of the 13 true cetacean sounds and their corresponding bionic signals are highly similar. Therefore, the camouflage ability of the synthesized bionic signals is very high.

TABLE 2. PCC results between 13 true cetacean sounds and their corresponding bionic signals.

Number	True cetacean sound	Bionic signal	PCC result
1	T_cf1	B_cf1	0.9827
2	T_cf2	B_cf2	0.9754
3	T_up1	B_up1	0.9984
4	T_up2	B_up2	0.9993
5	T_down1	B_down1	0.9973
6	T_down2	B_down2	0.9968
7	T_concave1	B_concave1	0.9998
8	T_concave2	B_concave2	0.9994
9	T_convex1	B_convex1	0.9900
10	T_convex2	B_convex2	0.9997
11	T_sine1	B_sine1	0.9996
12	T_sine2	B_sine2	0.9990
13	C_complex	B_complex	0.9997

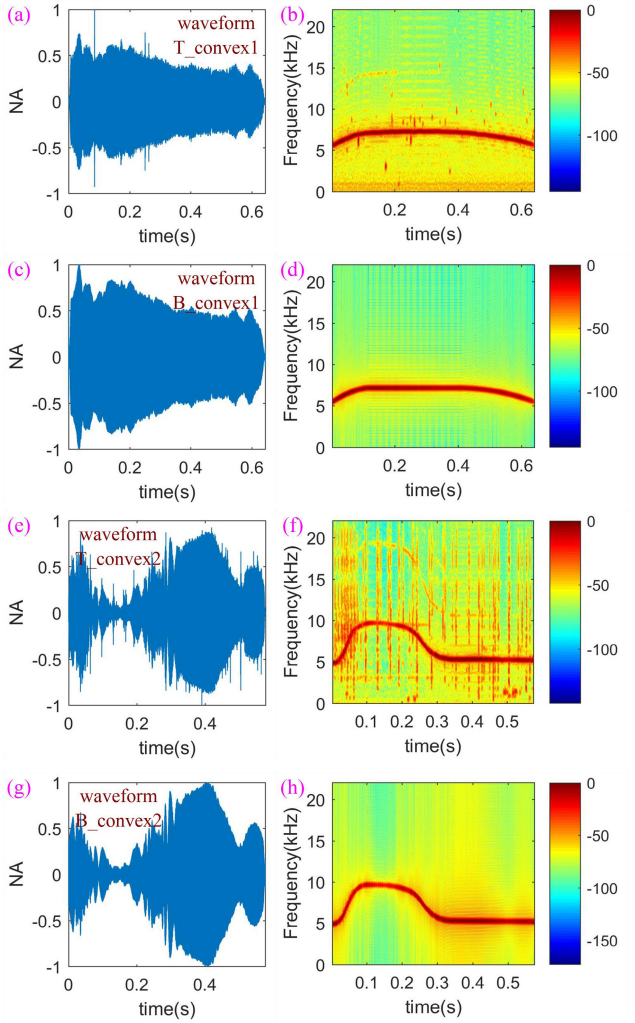

FIGURE 18. (a) The convex tonal sounds T_convex1. (b) The TFS of T_convex1. (c) The bionic signal B_convex1. (d) The TFS of B_convex1. (e) The convex tonal sounds T_convex2. (f) The TFS of T_convex2. (g) The bionic signal B_convex2. (h) The TFS of B_convex2.

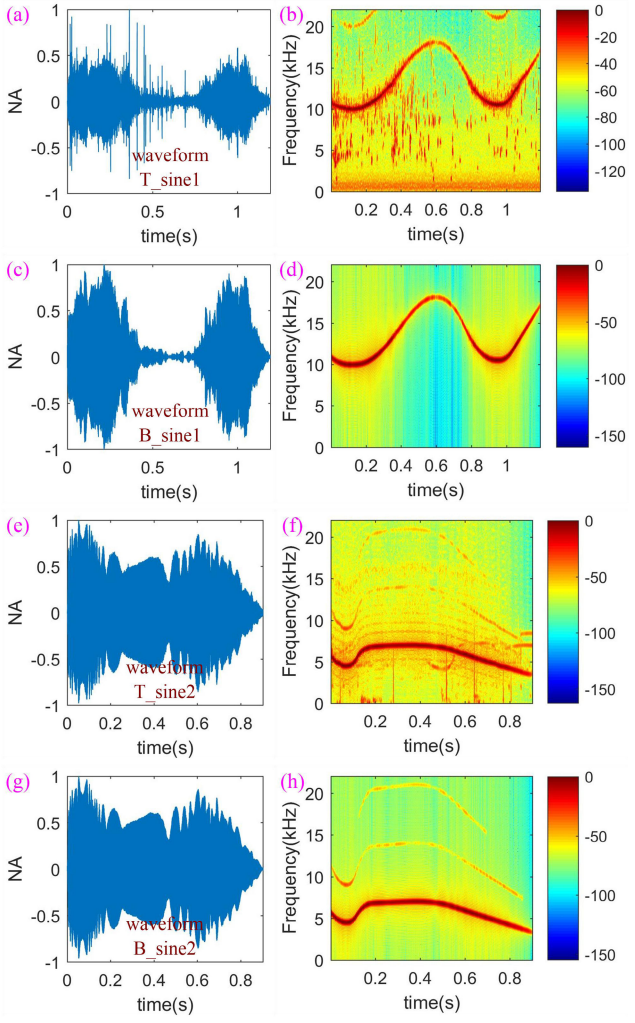

FIGURE 19. (a) The sine tonal sounds T_sine1. (b) The TFS of T_sine1. (c) The bionic signal B_sine1. (d) The TFS of B_sine1. (e) The sine tonal sounds T_sine2. (f) The TFS of T_sine2. (g) The bionic signal B_sine2. (h) The TFS of B_sine2.

D. MODULATION OF CETACEAN TONAL SOUNDS

In the fourth experiment, we examine the modification performance of the proposed method.

Here we take the upsweep tonal sound T_up1 (shown in Fig. 15(a)-(b)) as an example and construct its corresponding bionic signal B_up3. Under the condition of ensuring a good camouflage ability for B_up3, the parameters of the B_up3 are modified to improve its ASD and UAC performance. Furthermore, for radar, sonar and acoustic communication signal design, range resolution (RR), range sidelobe level (RSL), velocity resolution (VR), and Doppler tolerance (DT) are four key performance indicators, and they are obtained by the ambiguity function (AF) [38].

For ASD and UAC applications, when $B/f_o < 0.01$, the signal considered to be narrowband [39], where B is the bandwidth and f_o is the center frequency of the signal. Based on this criterion, it can be seen that the tonal sound T_up1 is wideband. Therefore, the wideband ambiguity function (WAF) [40]–[42] is used to examine the four key indicators above. The WAF can be defined as follows

$$WAF_S(\eta, \tau) = \sqrt{\alpha} \int s(t) s^*(\eta(t-\tau))\, dt, \tag{36}$$

where $\eta = (c-v)/(c+v) \approx 1 - 2v/c$ is the Doppler scale factor, $\tau = 2R/c$ is the propagation time delay, R is the target range, '$*$' is the complex conjugate operator, and c is the sound speed in water. Besides, for ASD applications, v is the relative speed between the sonar system and the target, and for UAC applications, v is the relative speed between the acoustic signal transmitter and the receiver.

The TF expression $f_{PO}(t)$ shown in (15) is chosen to construct B_up3. Therefore, the contour of B_up3 can be adjusted by modifying five parameters, which are carrier frequency f_C, bandwidth B, duration T, curvature adjustment factor α and slope adjustment factor k. By modifying these parameters, we found that increasing the value of B can improve the RR, RSL and VR of B_up3, while parameters α and k are related to the DT of B_up3. The parameter value of the tonal sound T_up1 and the bionic signal B_up3 are

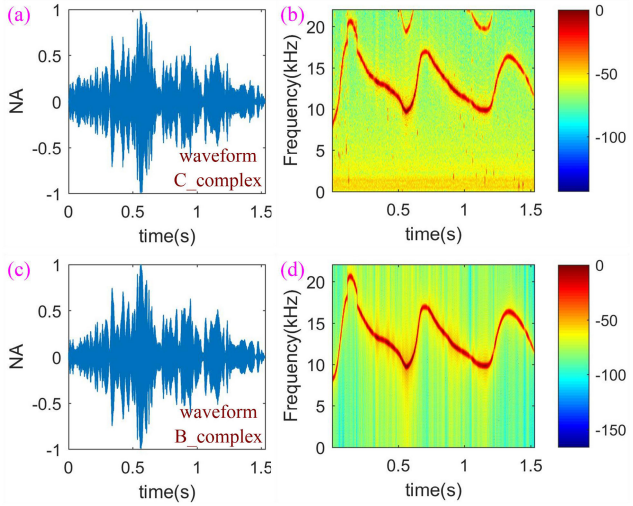

FIGURE 20. (a) The complex cetacean sound C_complex. (b) The TFS of C_complex. (c) The bionic signal B_complex. (d) The TFS of B_complex.

given in Table 3, where it can be seen that the frequency range of B_up3 (6.8 kHz to 10.3 kHz) is slightly expanded by 1 kHz based on that of T_up1 (6.8 kHz to 9.3 kHz). Moreover, the duration of B_up3 is slightly increased by 3ms based on that of T_up1.

TABLE 3. Parameters of tonal sound T_up1 and bionic signal B_up3.

Signal	Carrier frequency f_C (kHz)	Bandwidth B (kHz)	Duration T (ms)	Factor α	Factor k (kHz/s)
T_up1	6.8	2.5	579.6		
B_up3	6.8	3.5	582.6	1.6	1.8

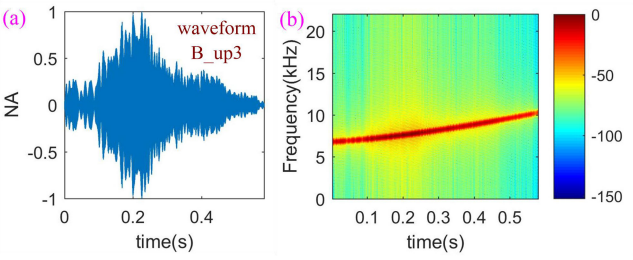

FIGURE 21. (a) The bionic signal B_up3. (b) The TFS of B_up3.

The waveform and TFS of B_up3 are shown in Fig. 21(a)-(b). By comparing Fig. 21(a)-(b) and Fig. 15(a)-(b), it can be seen that B_up3 can match T_up1 very well. Based on (35), we can obtain the PCC between B_up3 and T_up1 $r_{TB} = 0.9985$, which means that the contours of T_up1 and B_up3 are highly similar. Therefore, the camouflage ability of the synthesized bionic signal B_up3 is very high.

The RR, RSL, VR, and DT of T_up1 and B_up3 are shown in Table 4, where the change of RR is $(0.2716 - 0.5100)/0.5100 \times 100\% \approx -46.75\%$. Similarly, the changes of RSL, VR and DT are -40.31%, -61.18% and 1800%, respectively.

TABLE 4. Four key indicators of tonal sound T_up1 and bionic signal B_up3.

	RR(m)	RSL(dB)	VR(m/s)	DT(m/s)
T_up1	0.5100	-16.92	0.0850	0.7500
B_up3	0.2716	-23.74	0.0330	14.25
Change	-46.75%	40.31%	-61.18%	1800%

It can be seen that these four performance indicators of the bionic signal B_up3 are significantly improved compared to those of the tonal sound T_up1. For visualization, the WAF diagrams of the two signals are shown in Fig. 22.

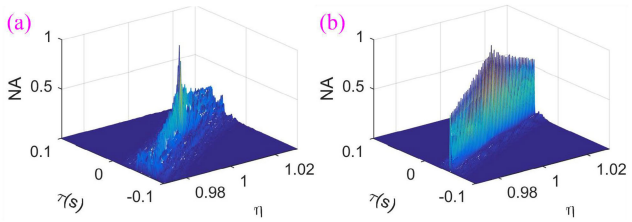

FIGURE 22. (a) WAF diagram of the true tonal sound T_up1. (b) WAF diagram of the bionic signal B_up3.

It is well-known that, for ASD applications, a higher RR and a lower RSL lead to high-accuracy range measurement, a higher VR indicates a high-accuracy speed measurement, and a larger DT allows range measurement for high-velocity targets. On the other hand, for UAC applications, RR and RSL correspond to time resolution (TR) and time sidelobe level (TSL), and a higher TR and a lower TSL results indicate a high-accuracy time measurement, while a higher DT allows effective UAC when the acoustic transmitter (or receiver) moves at a high speed. Based on the above analysis and results, it can be seen that by slightly modifying the parameters of the synthesized bionic signals, we can obtain bionic signals with both high camouflage ability and good detection and communication performance.

V. CONCLUSION

In this paper, based on the analysis of the acoustic characteristics of tonal sounds, two bionic signal models and their corresponding sub-models have been developed to match various TF structures of cetacean tonal sounds. Associated with the proposed bionic signal models, a piecewise construction strategy was developed to realize high-similarity mimicry of most tonal sounds and some complex cetacean sounds, such as signature whistle. The bionic signal models and their corresponding sub-models have exact and closed-form mathematical expressions, and together with the effective piecewise construction strategy, they provide the following benefits, as demonstrated by extensive design examples:

(1) The synthesized bionic signal waveforms are very close to the true cetacean tonal sounds, which can be used for the construction of high camouflage bionic signal waveforms.

(2) Most cetacean tonal sounds and some cetacean sounds (even though it has a complex TF structure) can be imitated with high similarity.
(3) The parameters (time domain envelope, frequency distribution and TF shape) of the synthesized bionic signals can be conveniently adjusted, which is very beneficial for the following two aspects: 1) generate other similar bionic signals, 2) change the detection and communication performance of bionic signals by felicitously adjusting the parameters of signal models.

Compared with the conventional methods [12]–[16], [24], [25], the proposed one cannot only achieve high camouflage ability, but also obtain high detection and communication performance for covert ASD and UAC through proper parameter adjustments. Moreover, the proposed method can also be employed for the construction of cetacean sound database and behaviour research of cetaceans.

REFERENCES

[1] S. J. Lourey, "Frequency hopping waveforms for continuous active sonar," in *Proc. IEEE Int. Conf. Acoust., Speech Signal Process. (ICASSP)*, Apr. 2015, pp. 1832–1835.
[2] Y. Chen, J. Liu, and X. Xu, "Optimization of energy consumption and covert communication for multi-hop underwater acoustic cooperative networks," (in Chinese), *J. Xiamen Univ. Nat. Sci.*, vol. 57, no. 1, pp. 112–117, Jan. 2018.
[3] M. I. Stanciu, S. Azou, and A. Serbanescu, "On the blind estimation of chip time of time-hopping signals through minimization of a multimodal cost function," *IEEE Trans. Signal Process.*, vol. 59, no. 2, pp. 842–847, Feb. 2011.
[4] J. Marszal and R. Salamon, "Detection range of intercept sonar for CWFM signals," *Arch. Acoust.*, vol. 39, no. 2, pp. 215–230, Mar. 2015.
[5] J. Marszal, R. Salamon, and L. Kilian, "Application of maximum length sequence in silent sonar," *Hydroacoustics*, vol. 15, pp. 143–152, 2012.
[6] R. S. Lynch, P. K. Willett, and J. M. Reinert, "Some analysis of the LPI concept for active sonar," *IEEE J. Ocean. Eng.*, vol. 37, no. 3, pp. 446–455, Jul. 2012.
[7] S. P. Van IJsselmuide and S. P. Beerens, "Detection and classification of marine mammals using an LFAS system," *Can. Acoust.*, vol. 32, no. 2, pp. 93–106, Jun. 2004.
[8] A. Papandreou-Suppappola and S. B. Suppappola, "Analysis and classification of time-varying signals with multiple time-frequency structures," *IEEE Signal Process. Lett.*, vol. 9, no. 3, pp. 92–95, Mar. 2002.
[9] J.-J. Jiang, L.-R. Bu, F.-J. Duan, X.-Q. Wang, W. Liu, Z.-B. Sun, and C.-Y. Li, "Whistle detection and classification for whales based on convolutional neural networks," *Appl. Acoust.*, vol. 150, pp. 169–178, Jul. 2019.
[10] J.-J. Jiang, L.-R. Bu, X.-Q. Wang, C.-Y. Li, Z.-B. Sun, H. Yan, B. Hua, F.-J. Duan, and J. Yang, "Clicks classification of sperm whale and long-finned pilot whale based on continuous wavelet transform and artificial neural network," *Appl. Acoust.*, vol. 141, pp. 26–34, Dec. 2018.
[11] H. S. Dol, B. A. J. Quesson, and F. P. A. Benders, "Covert underwater communication with marine mammal sounds," in *Proc. Undersea Defence Technol. Eur.*, Glasgow, U.K., Jun. 2008, pp. 10–12.
[12] J. Severson, "Modeling and frequency tracking of marine mammal whistle calls," M.S. thesis, Massachusetts Inst. Technol., Cambridge, MA, USA, 2009.
[13] A. ElMoslimany, M. Zhou, T. M. Duman, and A. Papandreou-Suppappola, "A new signaling scheme for underwater acoustic communications," in *Proc. OCEANS-San Diego*, Sep. 2013, pp. 1–5.
[14] A. ElMoslimany, M. Zhou, T. M. Duman, and A. Papandreou-Suppappola, "An underwater acoustic communication scheme exploiting biological sounds," *Wireless Commun. Mobile Comput.*, vol. 16, no. 15, pp. 2194–2211, Oct. 2016.
[15] S. Liu, T. Ma, G. Qiao, L. Ma, and Y. Yin, "Biologically inspired covert underwater acoustic communication by mimicking dolphin whistles," *Appl. Acoust.*, vol. 120, pp. 120–128, May 2017.
[16] J. Jiang, Z. Sun, F. Duan, W. Liu, X. Wang, C. Li, L. Bu, X. Fu, T. Huang, and L. Ma, "Disguised bionic sonar signal waveform design with its possible camouflage application strategy for underwater sensor platforms," *IEEE Sensors J.*, vol. 18, no. 20, pp. 8436–8449, Aug. 2018.
[17] S. Liu, G. Qiao, Y. Yu, L. Zhang, and T. Chen, "Biologically inspired covert underwater acoustic communication using high frequency dolphin clicks," in *Proc. OCEANS-San Diego*, Sep. 2013, pp. 1–5.
[18] S. Liu, G. Qiao, A. Ismail, B. Liu, and L. Zhang, "Covert underwater acoustic communication using whale noise masking on DSSS signal," in *Proc. MTS/IEEE OCEANS Bergen*, Jun. 2013, pp. 1–6.
[19] S. Liu, G. Qiao, and A. Ismail, "Covert underwater acoustic communication using dolphin sounds," *J. Acoust. Soc. Amer.*, vol. 133, no. 4, pp. EL300–EL306, Apr. 2013.
[20] J. Jia-jia, W. Xian-quan, D. Fa-jie, F. Xiao, Y. Han, and H. Bo, "Bio-inspired steganography for secure underwater acoustic communications," *IEEE Commun. Mag.*, vol. 56, no. 10, pp. 156–162, Oct. 2018.
[21] J. Jiang, X. Wang, F. Duan, C. Li, X. Fu, T. Huang, L. Bu, L. Ma, and Z. Sun, "Bio-inspired covert active sonar strategy," *Sensors*, vol. 18, no. 8, p. 2436, Jul. 2018.
[22] J. Jiang, X. Wang, F. Duan, X. Fu, T. Huang, C. Li, L. Ma, L. Bu, and Z. Sun, "A sonar-embedded disguised communication strategy by combining sonar waveforms and whale call pulses for underwater sensor platforms," *Appl. Acoust.*, vol. 145, pp. 255–266, Feb. 2019.
[23] W. W. L. Au, "The sonar signal transmission system," in *The Sonar of Dolphins*. Cham, Switzerland: Springer, 1993, pp. 77–97.
[24] J. R. Buck, H. B. Morgenbesser, and P. L. Tyack, "Synthesis and modification of the whistles of the bottlenose dolphin, Tursiops truncatus," *J. Acoust. Soc. Amer.*, vol. 108, no. 1, pp. 407–416, 2000.
[25] C. Capus, Y. Pailhas, K. Brown, D. M. Lane, P. W. Moore, and D. Houser, "Bio-inspired wideband sonar signals based on observations of the bottlenose dolphin (Tursiops truncatus)," *J. Acoust. Soc. Amer.*, vol. 121, no. 1, pp. 594–604, Jan. 2007.
[26] C. Bazúa-Durán and W. W. L. Au, "The whistles of hawaiian spinner dolphins," *J. Acoust. Soc. Amer.*, vol. 112, no. 6, pp. 3064–3072, Dec. 2002.
[27] V. M. Janik, D. Todt, and G. Dehnhardt, "Signature whistle variations in a bottlenosed dolphin, tursiops truncatus," *Behav. Ecology Sociobiology*, vol. 35, no. 4, pp. 243–248, Oct. 1994.
[28] A. G. Taruski, "The whistle repertoire of the North Atlantic pilot whale (Globicephala melaena) and its relationship to behavior and environment," in *Behavior of Marine Animals*, vol. 1979. Cham, Switzerland: Springer, 1979, pp. 345–368.
[29] A. N. Gavrilov, R. D. McCauley, C. Salgado-Kent, J. Tripovich, and C. Burton, "Vocal characteristics of pygmy blue whales and their change over time," *J. Acoust. Soc. Amer.*, vol. 130, no. 6, pp. 3651–3660, Dec. 2011.
[30] L. J. May-Collado, I. Agnarsson, and D. Wartzok, "Phylogenetic review of tonal sound production in whales in relation to sociality," *BMC Evol. Biol.*, vol. 7, no. 1, p. 136, 2007.
[31] J. N. Matthews, L. E. Rendell, J. C. D. Gordon, and D. W. Macdonald, "A review of frequency and time parameters of cetacean tonal calls," *Bioacoustics*, vol. 10, no. 1, pp. 47–71, Jan. 1999.
[32] J. J. Dreher, "Linguistic considerations of porpoise sounds," *J. Acoust. Soc. Amer.*, vol. 33, no. 12, pp. 1799–1800, Dec. 1961.
[33] M. A. Calderon, "Probability density analysis of ocean ambient and ship noise," U.S. Navy Electron. Lab., San Diego, CA, USA, Tech. Rep. 1248, 1964.
[34] A. Papandreou-Suppappola, "Time-frequency processing: Tutorial on principles and practice," in *Applications in Time-Frequency Signal Processing*. Boca Raton, FL, USA: CRC Press 2002.
[35] Y. Wang, Z. Wang, B. Zhao, and L. Xu, "Parameters estimation of sinusoidal frequency modulation signal with application in synthetic aperture radar imaging," *J. Appl. Remote Sens.*, vol. 10, no. 2, p. 20502, 2016.
[36] V. M. Janik and P. J. B. Slater, "Context-specific use suggests that bottlenose dolphin signature whistles are cohesion calls," *Animal Behav.*, vol. 56, no. 4, pp. 829–838, Oct. 1998.
[37] H. Khayyam, "Stochastic models of road geometry and wind condition for vehicle energy management and control," *IEEE Trans. Veh. Technol.*, vol. 62, no. 1, pp. 61–68, Jan. 2013.
[38] M. Vespe, G. Jones, and C. J. Baker, "Lessons for radar," *IEEE Signal Process. Mag.*, vol. 26, no. 1, pp. 65–75, Jan. 2009.
[39] M. C. Wicks, E. Mokole, S. D. Blunt, R. S. Schneible, and V. J. Amuso, *Principles of Waveform Diversity and Design*. Rijeka, Croatia: SciTech, 2010.

[40] L. G. Weiss, "Wavelets and wideband correlation processing," *IEEE Signal Process. Mag.*, vol. 11, no. 1, pp. 13–32, Jan. 1994.
[41] J.-J. Jiang, X.-Q. Wang, F.-J. Duan, H. Yan, B. Hua, S.-X. Ma, C. Deng, L. Bu, Z. Sun, and C. Li, "An efficient algorithm for WBAF estimation based on linear interpolation and its estimation error," *Appl. Acoust.*, vol. 142, pp. 44–52, Dec. 2018.
[42] J. Jiang, X. Wang, F. Duan, W. Liu, L. Bu, F. Li, C. Li, Z. Sun, S. Ma, and C. Deng, "Study of the relationship between pilot whale (Globicephala melas) behaviour and the ambiguity function of its sounds," *Appl. Acoust.*, vol. 146, pp. 31–37, Mar. 2019.

JIAJIA JIANG (Senior Member, IEEE) was born in Hubei, China, in 1986. He received the B.S. degree from the Hebei Normal University and the M.S. and Ph.D. degrees from the State Key Lab of Precision Measuring Technology Instruments, Tianjin University, Tianjin, China, in 2011 and 2014, respectively.

He is currently an Associate Professor with the State Key Lab of Precision Measuring Technology Instruments, Tianjin University. His research interest include underwater acoustic detection, underwater acoustic communication, and array signal processing.

ZHONGBO SUN was born in Hubei, China, in 1993. He received the B.S. degree from Liaoning University, Shenyang, China, in 2016. He is currently pursuing the Ph.D. degree with the State Key Lab of Precision Measuring Technology and Instruments, Tianjin University.

His research interest focuses on the underwater acoustic detection and communication.

FAJIE DUAN was born in Hunan, China, in 1968. He received the M.S. degree from Tianjin University and the Ph.D. degree from the State Key Lab of Precision Measuring Technology Instruments, Tianjin University, Tianjin, China, in 1991 and 1994, respectively.

He has been a Professor with the State Key Lab of Precision Measuring Technology Instruments, Tianjin University, since 2004. He is the author or coauthor of over 120 articles and holds seven patents. His research interests include the design of the array system, array signal processing, and acoustic detection of marine. He was named the National New Century Excellent Talents of Ministry of Education, in 2005.

XIAO FU was born in Shandong, China, in 1990. He received the B.Eng. degree from Tianjin University, Tianjin, China, in 2013, where he is currently pursuing the Ph.D. degree with the State Key Lab of Precision Measuring Technology Instruments.

His research interest focuses on the underwater communication and detection.

XIANQUAN WANG received the B.S. degree from the State Key Lab of Precision Measuring Technology and Instruments, Tianjin University, in 2015, where he is currently pursuing the Ph.D. degree with the State Key Lab of Precision Measuring Technology and Instruments.

His research interest focuses on the underwater communication and detection.

CHUNYUE LI was born in Hebei, China, in 1993. She received the B.S. degree from Northeastern University, Shenyang, China, in 2016. She is currently pursuing the Ph.D. degree with the State Key Lab of Precision Measuring Technology Instruments, Tianjin University, Tianjin, China.

Her research interest focuses on the underwater acoustic detection and communication.

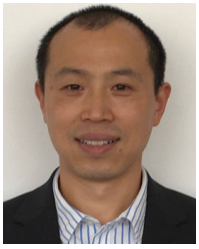

WEI LIU (Senior Member, IEEE) received the B.Sc. and L.L.B. degrees from Peking University, China, in 1996 and 1997, respectively, the M.Phil. degree from The University of Hong Kong, in 2001, and the Ph.D. degree from the School of Electronics and Computer Science, University of Southampton, U.K., in 2003.

He held a postdoctoral position at the Imperial College London. Since 2005, he has been with the Department of Electronic and Electrical Engineering, The University of Sheffield, U.K., as a Lecturer and then as a Senior Lecturer. He has authored over 230 journal and conference papers, three book chapters, and a research monograph about wideband beamforming *Wideband Beamforming: Concepts and Techniques* (Wiley, 2010). His research interests are in sensor array signal processing, blind signal processing, multivariate signal processing, and their various applications in wireless communications, radar, sonar, satellite navigation, human computer interface, and renewable energy exploitation.

LIN GAN (Member, IEEE) received the B.S. degrees from Tianjin University, Tianjin, China, in 2015, where she is currently pursuing the Ph.D. degree in instrument technology and science. Her research interest focuses on acoustic signal processing.